Peer-reviewed version available at *Materials* **2019**, *12*, 1681; doi:10.3390/ma12101681

Article

Research on Recognition Technology of Aluminum Profile Surface Defects Based on Deep Learning

Ruofeng Wei[2], Yunbo Bi[1,2,*]

[1] State Key Laboratory of Fluid Power and Mechatronic System, College of Mechanical Engineering, Zhejiang University, Hangzhou 310027, China

[2] Key Laboratory of Advanced Manufacturing Technology of Zhejiang Province, College of Mechanical Engineering, Zhejiang University, Hangzhou 310027, China

[*] Correspondence: zjubyb@zju.edu.cn

Abstract: Aluminum profile surface defects can greatly affect the performance, safety and reliability of products. Traditional human-based visual inspection is low accuracy and time consuming, and machine vision-based methods depend on hand-crafted features which need to be carefully designed and lack robustness. To recognize the multiple types of defects with various size on aluminum profiles, a multiscale defect detection network based on deep learning is proposed. Then, the network is trained and evaluated using aluminum profile surface defects images. Results show 84.6%, 48.5%, 96.9%, 97.9%, 96.9%, 42.5%, 47.2%, 100%, 100%, 43.3% average precision(AP) for the ten defect categories, respectively, with a mean AP of 75.8%, which illustrate the effectiveness of the network in aluminum profile surface defects detection. In addition, saliency maps also show the feasibility of the proposed network.

Keywords: aluminum profile surface defects; multiscale defect detection network; deep learning; average precision(AP); saliency maps

1. Introduction

Aluminum alloys have drawn more and more attention in aerospace engineering, automotive, and electronics industry, due to their low density, high specific strength, good corrosion resistance, and good recycling ability [1,2]. Aluminum profile is an application form of aluminum alloys, and the demand for it is extremely large because of the massive use of space-frame constructions in high-speed rail and auto body [3]. Therefore, surface quality of aluminum profiles have assumed significant importance. Any surface defects such as cracks and deformations will greatly affect the performance, safety and reliability of products. Traditionally, human-based visual inspection is a common detection method in manufacturing engineering. However, due to low sampling rate, low precision, poor real-time performance, fatigue, greatly influenced by artificial experience, and other adverse factors, the artificial inspection is not sufficient to guarantee the stability and accuracy of detection. In addition, the other methods based on various signals, like electrical signal and magnetic signal, were also utilized to detect the surface defects by many companies. ABB Metallurgy [4] developed the Decraktor detection unit P1 using the principle of multi-frequency eddy current testing. The device can suppress the influence of various interference noises, thereby improving the reliability of the steel plate detection. However, eddy current testing can only detect conductors and needs to be close to the surface being inspected. Besides, the rough surface affects the detection result and the penetration depth of eddy current detector is limited.

Peer-reviewed version available at Materials 2019, 12, 1681; doi:10.3390/ma12101681

Machine vision-based method for surface defect detection has an absolute advantage in terms of its safety, reliability, convenience and efficiency. It is an effective means to realize the automation and intellectualization of the manufacturing processes in steel and iron industry [5,6]. A typical machine vision-based defect detection method consists of light source, CCD camera, and image processing algorithms [7]. Many scholars have conducted significant research on image processing algorithms. However, there is not much literature about aluminum profile defect detection using machine vision technology. Nevertheless, the problem can be seen as defect detection in mental material, such as steel and iron, which has been studied for many years in computer vision.

Mathematical morphology is a technique of image analysis based on set theory, topology, and random functions. Dupont *et al*. [8] proposed a method using the cost matrix theory based on mathematical morphology, and the K-nearest neighbor(KNN) [9] classifier to detect eight kinds of defects on flat steel products. Spatial filtering is a image processing method that directly manipulates the pixels in an image. The gradient filters, like Sobel, Robert, Canny, and Laplacian filters are popular tools to detect points, lines and edges in spatial filtering. Guo *et al*. [10] used the Sobel gradient operator and Fisher discriminant to detect defects on the steel surface. Moreover, Wu *et al*. [11] adopted a method based on fast Fourier transform(FFT) combined with a local border search algorithm for the recognition of hot-rolled steel strips. In [12], Yazdchi *et al.* applied a multifractal-based segmentation method to detach the region of defects from images, and then extracted ten features from the detected region for classification. A method in [13] using the Markov random field for texture analysis combined with a KNN classifier was used for classification of steel surface defects.

Although traditional machine vision-based methods using the CCD camera and image processing algorithms achieved the automatic detection of surface defects, the hand-designed features [14] used in the defect detection needed to be carefully designed by a programmer who well understands the domain of the task, which lacks robustness and is not conducive to the identification, classification and detection of surface defects.

In recent years, due to the advances of artificial intelligence and deep learning, more concretely convolutional neural network(CNN) [15], the quality of image classification, object detection and face recognition has been rapidly developed. Deep learning which is based on artificial neural network discovers the distributed representation of its input data by transforming the data and low-level features into a more abstract and composite representation; the CNN can learn highly abstract and invariable features from large training dataset automatically, rather than constructing low level features artificially, therefore, it can be robustly adapted to various computer vision tasks.

In 2012, as the winner of the ImageNet Large Scale Visual Recognition Challenge (ILSVRC) [16,17], Krizhevsky *et al*. [14] rekindled interests in CNN by firstly using deeper and wider networks in computer vison tasks. In [18], Girshick *et al*. proposed region-based CNN(R-CNN) which uses selective search[19] to generate around 2000 region proposals and "AlexNet"[14] to extract features, and a set of SVMs [20] and a regression model to classify and localize objects. However, the R-CNN is computationally expensive and slow, and not widely used in actual applications because it requires thousand of forward computations from the CNN to perform object detection for a single image. To address the drawbacks of R-CNN, Fast R-CNN [21] was developed by Girshick *et al*. Fast R-CNN only performs CNN forward computation on the image as a whole, so it shows higher speed and accuracy than R-CNN. Despite the better performance, Fast R-CNN generates many proposed regions through an external method like selective search which is time consuming. In 2016, a region proposal network(RPN) was presented to generate nearly cost-free region proposals in [22], and Ren *et al*. introduced the Faster R-CNN by combining the RPN and Fast R-CNN for object detection. The Faster R-CNN reduces the computational cost through sharing convolutional

features between RPN and Fast R-CNN. Moreover, the novel RPN also improves the overall precision of object detection.

In computer vision, the objects of deep learning are often natural images, including pedestrians, vehicles, animals and human faces, etc., but there are few studies on aluminum profile surface defects detection using the deep learning. Therefore, in this paper, we propose a multiscale defect detection network for detecting the aluminum profile surface defects, which was based on the use of CNNs. The network is based on Faster R-CNN and feature pyramid network(FPN) [23], and can effectively detect surface defects with various scale.

The rest of this paper is organized as follows. In Section 2, the dataset for training and evaluating the network is described. The multiscale defect detection network is presented in Section 3, including the architecture of the network and how to train the network. Section 4 gives a experiment for training the network, including the implementation details of the experiment and the loss in the training process. In Section 5, the evaluation results of the network are presented. The paper ends with a summary of the major findings in Section 6.

2. Dataset

2.1. Dataset of the network

Figure **1** shows the images of aluminum profile surface defects for training and evaluating the multiscale defect detection network, and the resolution of each image is 2560x1920 pixels. The aluminum profile surface defects dataset is from [24].There are ten types of defects on aluminum profile: Non-conductive(NC), Scratch, Corner Leak(CL), Orange Peel(OP), Leakage, Jet, Paint Bubble(PB), Crater, Parti-color(PC), Dirty Point(DP), and the defect is marked with a ground truth box which is like the red rectangle in Figure **Error! Reference source not found.**. The total number of images with defects is 3005, including 2776 images with single type defect and 229 images with multiple types of defects. To obtain the training dataset, images are randomly chosen from the overall dataset so that the training dataset contained about 90% of images of each defect type. Thus, there are 2705 images for training and 300 images for testing. Figure **2** shows the number of images with defects in each category.

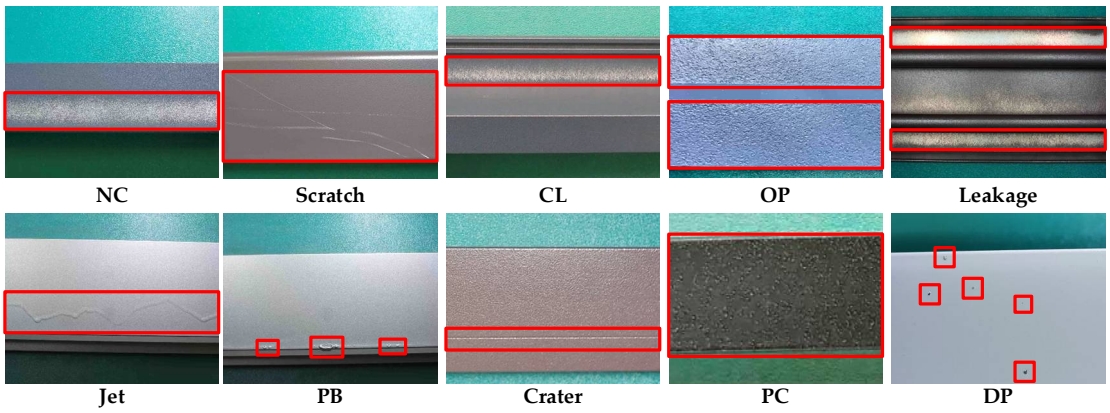

Figure 1. Images of aluminum profile surface defects.

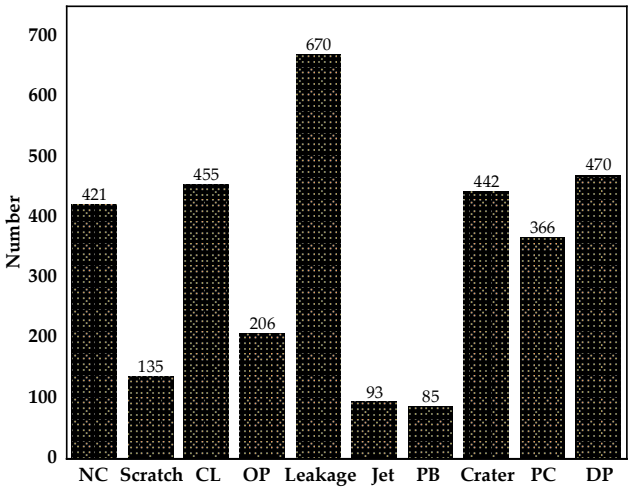

Figure 2. Diagram of the number of images with defects in each category.

As can be seen in Figure **Error! Reference source not found.**, some defects are particularly small, such as PB and DP, and some defects are extremely narrow and long, like Crater. These defects with abnormal size increase the difficulty of defect detection.

2.2. Data augmentation

Convolutional neural network(CNN), especially deep ones, is likely to be prone to overfitting when training dataset is small. The aluminum profile surface defects dataset, we use, comprises only several thousands samples, which may not fully sustain the training of deep CNNs. Moreover, it is time-consuming and laborious to make large training dataset with defect location annotations by professional annotators.

Therefore, a data augmentation technique [25] is performed over the original defect dataset aiming the dataset expansion. To do so, each image and corresponding ground truth boxes are passed through some transformations: vertical flip, horizontal flip and horizontal vertical flip(shown in Figure **Error! Reference source not found.**).

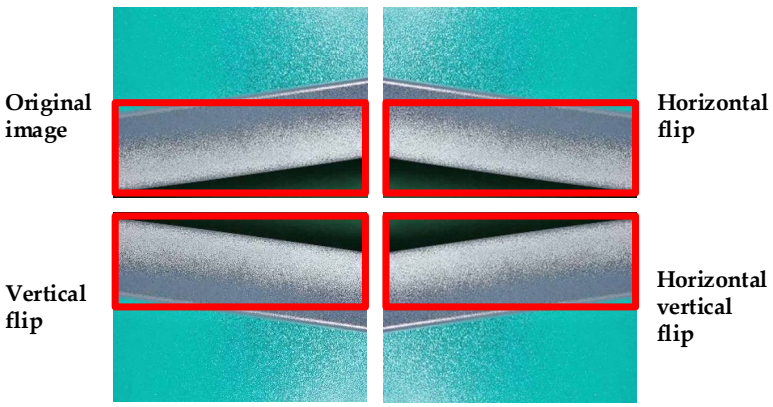

Figure 3. Data augmentation.

3. Method

To classify and localize defects on the aluminum profile surface, the multiscale defect detection network based on Faster R-CNN is proposed. The overall schematic architecture of the network is presented in Figure **Error! Reference source not found.**. The Faster R-CNN system was composed of Feature Extraction Network(FEN), Region Proposal Network(RPN), Region-of-Interesting(ROI) Pooling, and Classification and Regression Layer. Considering the

Preprints (www.preprints.org) | NOT PEER-REVIEWED | Posted: 29 April 2019 doi:10.20944/preprints201904.0322.v1

Peer-reviewed version available at Materials 2019, 12, 1681; doi:10.3390/ma12101681

characteristics of surface defects of aluminum profiles, the idea of feature fusion from FPN is added to the basic Faster R-CNN to improve defect detection performances. The details of the multiscale defect detection are explained in this section.

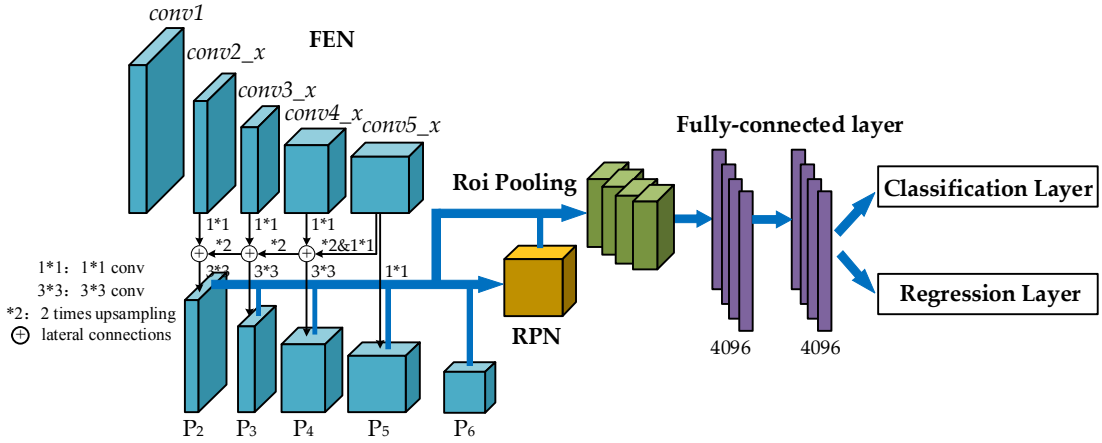

Figure 4. Architecture of the multiscale defect detection network.

3.1. Feature Extraction Network

FEN is a large CNN which can automatically extract high-level features from input images. In this study, we use ResNet101 [26] to obtain high-level and semantically strong features. The basic structure of the ResNet101 is a bottleneck which solves a network performance degradation problem and leads the CNN model deeper than ever. As depicted in Figure **Error! Reference source not found.**, the bottleneck contains three convolutional layers: 1x1, 3x3, and 1x1 convolutional layer, which is followed by a "Relu" activation function [27], respectively, and "shortcut connections" which are those skipping one or more layers and map input features directly to output without extra parameter.

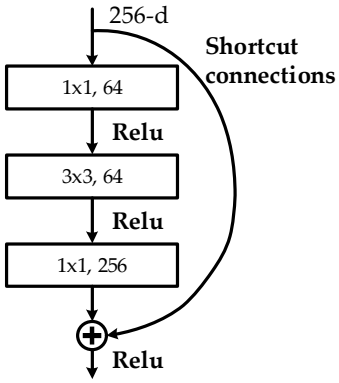

Figure 5. Structure of the *bottleneck*.

The detailed architecture of the ResNet101 for ImageNet is summarized in Table **Error! Reference source not found.**. The network is composed of *conv1*, *pool*, *conv2_x*, *conv3_x*, *conv4_x*, *conv5_x*, average pool, 1000-d fully connected layer(1000-d fc). The output of fully connected layer is fed to a 1000 way softmax which can produce a probability distribution over 1000 classes. When applied to extract feature maps, we only use the *conv1*, *pool*, *conv2_x*, *conv3_x*, *conv4_x* and *conv5_x*. The *conv2_x*, *conv3_x*, *conv4_x* and *conv5_x* are constructed by *bottleneck* stacked upon each other, and the number of *bottleneck* of each section is shown in Table **Error! Reference source not found.**. Because of the "very deep" network, high-level semantic features that facilitate subsequent recognition can be obtained from the *conv5_x*.

Preprints (www.preprints.org) | NOT PEER-REVIEWED | Posted: 29 April 2019 doi:10.20944/preprints201904.0322.v1

Peer-reviewed version available at Materials 2019, 12, 1681; doi:10.3390/ma12101681

Table 1. Architecture of the ResNet101.

Layer name	Output size	101-layer
*conv*1	112×112	7x7, 64, stride 2
pool	56×56	3x3 max pool, stride 2
*conv*2_*x*	56×56	$\begin{bmatrix} 1\times1, & 64 \\ 3\times3, & 64 \\ 1\times1, & 256 \end{bmatrix}\times3$
*conv*3_*x*	28×28	$\begin{bmatrix} 1\times1, & 128 \\ 3\times3, & 128 \\ 1\times1, & 512 \end{bmatrix}\times4$
*conv*4_*x*	14×14	$\begin{bmatrix} 1\times1, & 256 \\ 3\times3, & 256 \\ 1\times1, & 1024 \end{bmatrix}\times23$
*conv*5_*x*	7×7	$\begin{bmatrix} 1\times1, & 512 \\ 3\times3, & 512 \\ 1\times1, & 2048 \end{bmatrix}\times3$
	1×1	average pool, 1000-d fc, softmax

However, the high-level feature maps are usually low-resolution; so when small scale defects on the aluminum profile are mapped into high-level features, the representational capacity for these defects detection can be weakened. The idea of feature fusion is to combine low-resolution, semantically strong features with high-resolution, low-level features. As shown in Figure **Error! Reference source not found.**, the architecture of feature fusion in the multiscale defect detection network adopts a top-down pathway and lateral connections. The top-down pathway produces higher resolution and semantically stronger features by upsampling semantically stronger, but lower resolution feature maps to nearest lower level features' scale, and then these features are added to the nearby low-level features via lateral connections. Therefore, a set of multiscale feature maps: {P_2, P_3, P_4, P_5} in which all levels are semantically strong are generated. In addition, an extra feature map P_6 which is a simply two stride subsampling of P_5 is added to the output feature maps. Then, it is worth noting that the feature maps {P_2, P_3, P_4, P_5, P_6} will be transmitted to RPN and only {P_2, P_3, P_4, P_5} will be input into ROI pooling.

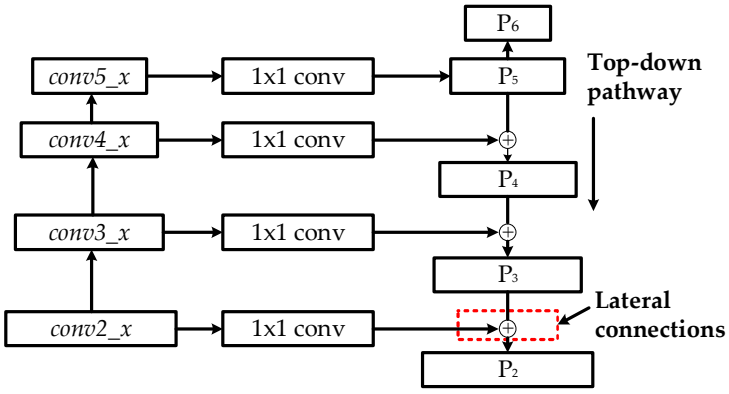

Figure 6. Architecture of feature fusion in the multiscale defect detection network.

3.2. Region Proposal Network

After feature fusing, RPN can generate region proposals or regions of interest(roi), which are rectangular regions surrounding defects, including the probability of being foreground(containing defects) in each proposal. The schematic structure of a improved RPN

Preprints (www.preprints.org) | NOT PEER-REVIEWED | Posted: 29 April 2019 doi:10.20944/preprints201904.0322.v1

Peer-reviewed version available at Materials 2019, 12, 1681; doi:10.3390/ma12101681

is presented in Figure Error! Reference source not found.. The improved RPN is a fully convolutional network, which is naturally implemented with a 3x3 convolutional(conv) layer followed by two sibling 1x1 convolutional(conv) layers for classification and regression. Concretely, we attach the fully convolutional network(3x3 conv and two 1x1 convs) to each feature map output by FEN, and then several vectors containing estimate probability of defect / not-defect for each anchor and prediction coordinate transformation from anchors to region proposals are generated.

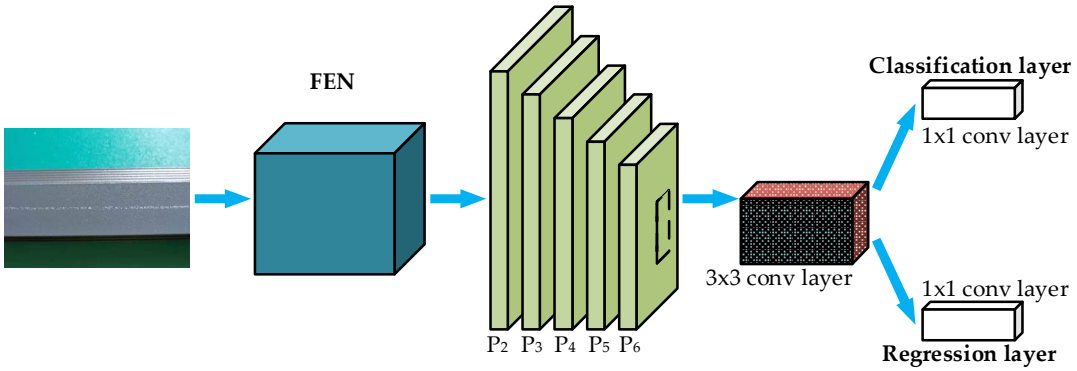

Figure 7. Structure of the improved RPN.

Anchors play an important role in the improved RPN. An anchor is a reference box, determined by upper left and lower right coordinates: (x_1, y_1) and (x_2, y_2), as shown in Figure Error! Reference source not found.a. The anchor which is previously assigned on the input image transforms the defect detection problem into whether the anchor surrounds any defects and how far away is the defect from the anchor(shown in Figure Error! Reference source not found.b). Based on the work of Lin *et al*. [23], we defines the anchors to have areas of $\{32^2, 64^2, 128^2, 256^2, 512^2\}$ pixels corresponding to $\{P_2, P_3, P_4, P_5, P_6\}$ in the improved RPN. Moreover, the anchor in each feature map has three aspect ratios: {1:2, 1:1, 2:1}. In the improved RPN, there are 15 kinds of anchors, and approximately 306900 anchors set on the input image.

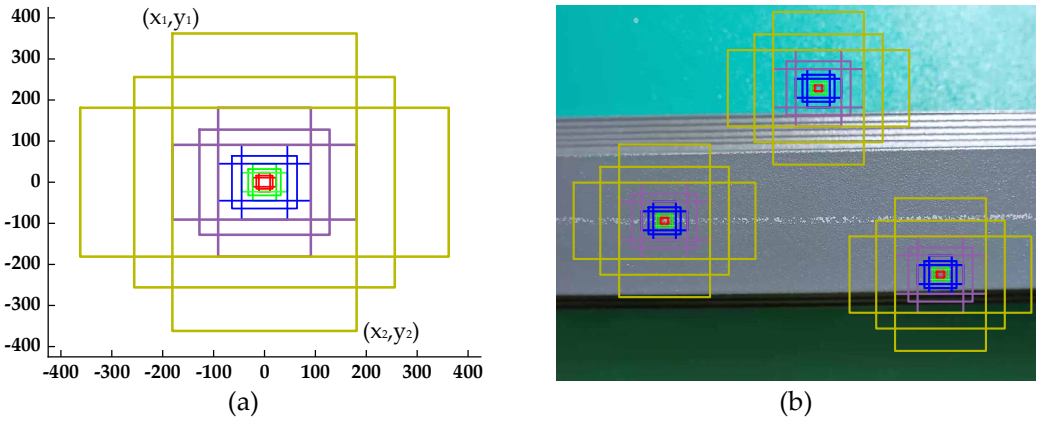

Figure 8. **(a)** 15 kinds of anchors; **(b)** Anchors set on the input image.

Although the improved RPN could create a large number of anchors, and some of which may be close to defects, these anchors provide coarse localization and need to be refined. The regression layer is a simple, inexpensive technique which can compensate for the anchors' weakness at localization. Concretely, it attempts to learn a transformation d*(A) that maps the anchors to the region proposal. As described in Figure Error! Reference source not found.a, A is the anchor, G is the ground truth box, and G' is the predicting region proposal, which are

Preprints (www.preprints.org) | NOT PEER-REVIEWED | Posted: 29 April 2019 doi:10.20944/preprints201904.0322.v1

Peer-reviewed version available at Materials 2019, 12, 1681; doi:10.3390/ma12101681

specified as a set of center coordinates and a width and height in pixels, where A = (A_x, A_y, A_w, A_h). Thus, the transformation d*(A) could transform A into G' which is more closer to G and better captures the defect:

$$\begin{aligned} G'_x &= A_w d_x(A) + A_x \\ G'_y &= A_h d_y(A) + A_y \\ G'_w &= A_w \exp(d_w(A)) \\ G'_y &= A_h \exp(d_h(A)) \end{aligned} \tag{1}$$

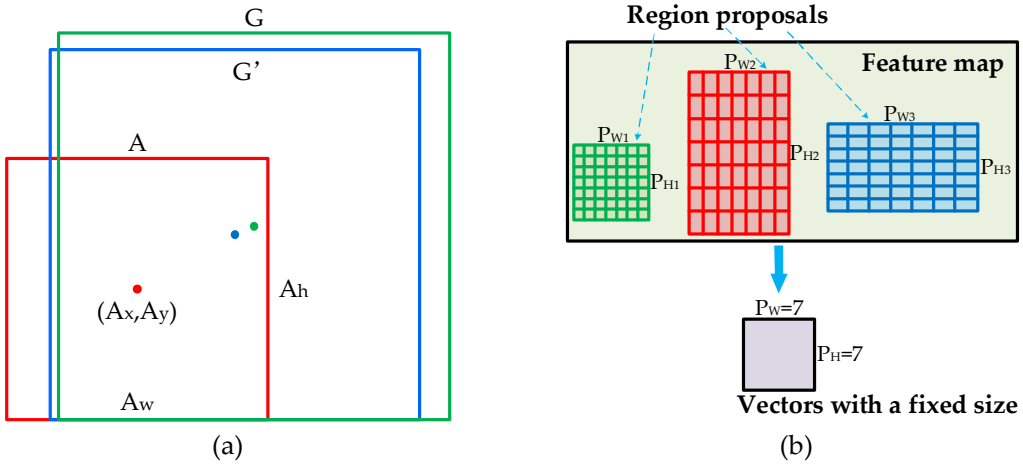

Figure 9. **(a)** The schematic diagram of the regression layer; **(b)** ROI pooling.

3.3. ROI Pooling

The region proposals output from the improved RPN have different dimensions, and the input of final classification and regression layer need to be the same size, so the purpose of ROI pooling is to perform max pooling to convert the features inside any proposals into vectors with a fixed size(e.g., 7x7). The specific operation of ROI pooling is shown in Figure **Error! Reference source not found.**b. Firstly, the region proposals with different size are divided into equal-sized sections, such as 7x7; then, the max value in each section is output, and fixed-size vectors can be obtained.

In addition, the region proposal with (x_1, y_1) and (x_2, y_2) need to be mapped to the feature maps before the operation ROI Pooling. There are four feature maps {P_2, P_3, P_4, P_5} input to ROI pooling, so it is important to determine which feature map the region proposal belongs to. According to Lin [23], we assign a region proposal of width w and height h(on the input image) to the feature map P_k by:

$$k = 4 + \log_2(\sqrt{wh}/224) \tag{2}$$

Intuitively, if the region proposal's scale is 512x512, it should be mapped to P_5. The mapping method is to reduce coordinates of the anchor to the downsampling multiple of the input image to the feature map. For example, we define the anchor with area of 512^2 pixels on P_5 feature map. Therefore, one anchor which is center at the input image with scale: {-256, 256, 256, -256 } is {-8, 8, 8, -8} when mapped to P_5.

3.4. Classification and Regression Layer

The Classification and Regression layer are composed of fully-connected layers. For the classification layer, it outputs a vector with the predicting probability of 11 classes(10 defects plus 1 background class); the regression layer outputs four parameters for each class to refine

Peer-reviewed version available at Materials 2019, 12, 1681; doi:10.3390/ma12101681

the region proposals again. Before the final classification and regression layer, there are two hidden, 1024-d fully connected layers which map the learned features to the sample space for classification and regression.

3.5. Network Training

The multiscale defect detection network is composed of the architecture of the network and weights of the convolutional layers. When the design of network structure is completed, we need to obtain the optimal weights of the convolutional layers. Network training is a process that realizes the optimization of weights and leads the prediction of the network approximating to the truth of inputs, and it consists of forward propagation and backward propagation. Forward propagation is the calculation and storage of intermediate variables(including outputs) for the network in the order from input to output. Backward propagation refers to the method of calculating the losses(the difference between outputs and the truth of inputs) of the network and updating the weights using the gradient from the losses. The losses of the multiscale defect detection network are from the improved RPN and the Classification and Regression layer. In the training, the selection of the losses is extremely significant.

The improved RPN is trained end-to-end, for both classification and regression layer. We use the multitask loss L in Fast R-CNN[21] to train the improved RPN:

$$L(p_i, t_i) = \frac{1}{N_{cls}} \sum L_{cls}(p_i, p_i^*) + \lambda \frac{1}{N_{reg}} \sum_i p_i^* \times L_{reg}(t_i, t_i^*) \tag{3}$$

where i is the index of an anchor in a mini-batch, and in the classification loss p* and p are the ground truth label and predicted probability of being defects in the anchor, respectively. In the regression loss, t_i and t_i^* are vectors representing the geometrical difference between the anchor and the predicting region proposal, as well as the anchor and the ground truth box, and ti* is calculated as:

$$\begin{aligned} t_x^* &= (G_x - A_x)/A_w \\ t_y^* &= (G_y - A_y)/A_h \\ t_w^* &= \log(G_w / A_w) \\ t_h^* &= \log(G_h / A_h) \end{aligned} \tag{4}$$

Additionally, the classification loss is calculated as:

$$L_{cls} = \sum_i -p_i^* \times \log(p_i) - (1 - p_i^*) \times \log(1 - p_i) \tag{5}$$

The regression loss is calculated as:

$$L_{reg} = \sum_i smooth_{L1}(t_i^* - t_i)$$

$$\left(smooth_{L1}(x) = \begin{cases} 0.5x^2 & \text{if } |x| < 1 \\ |x| - 0.5 & \text{otherwise} \end{cases} \right) \tag{6}$$

Moreover, we use the same loss as the improved RPN to train the Classification and Regression layer, which are also trained end-to-end.

4. Experiments

4.1. Implementation Details

In the research on recognition of aluminum profile surface defects, all experiments are performed using Python 3.5, PyTorch as the deep learning library, cuda 9.1 and cudnn 5.1 on Google Cloud Platform with a 8 GB memory NVIDA Tesla K80 graphics processing unit(GPU). While training the multiscale defect detection network, we apply scaling of 960 on the shorter side of input images(with the resolution of 2560x1280), and then normalize each

Preprints (www.preprints.org) | NOT PEER-REVIEWED | Posted: 29 April 2019 doi:10.20944/preprints201904.0322.v1

Peer-reviewed version available at Materials 2019, 12, 1681; doi:10.3390/ma12101681

image, by making it have fixed means and variances. When calculating the losses of the network, λ=1 is used both in RPN's and Classification and Regression Layer's loss function. In addition, weights of the network are improved by stochastic gradient descent(SGD), including a learning rate of 0.001, momentum of 0.9, and weight decay of 0.0005. In the training of the network, we propose to use 1 in batch size(batch means the number of input images), and 50 epochs to improve the performance(epoch means the number of the network is trained).

When evaluating the performance of an object detection network, average precision(AP) is often used. Detailed descriptions of AP can be seen in the paper by Everingham *et al*. [28]. In the multiscale defect detection, we use mean AP(mAP) which is defined as the average of calculated APs for ten types of defects to evaluate.

4.2. Loss in Network Training

During the process of network training, it is necessary to visualize the loss on the training dataset in time. Whether the defect detection network is effective can be judged by the trend of the loss curve. Moreover, the loss can guide the adjustment of parameters in the network, including training epoch, learning rate, weight decay and structural optimization. The total losses of the multiscale defect detection network consist of the classification loss and regression loss in RPN, and classification loss and location loss in Classification and Regression Layer. In the training, the various losses can be represented by total_loss, rpn_cls_loss, rpn_box_loss, cls_loss and loc_loss, respectively.

The loss curves during the training are shown in Figure **Error! Reference source not found.**. In this study, the network is trained on all training dataset in each epoch, and the various losses of the network are recorded every 50 steps(one step equals to an image), so there are 2700 iterations totally in all loss curves(one iteration equals to 50 steps). As shown in Figure **Error! Reference source not found.**, all kinds of loss curves display a downward trend, and the loss decreases greatly at the beginning of training, indicating that the learning rate is appropriate and the gradient descent is carried out. Then, the loss curves tend to be stable after training to a certain epoch, which indicates that the network starts to converge. Thus, the parameters we selected in Section 4.1 are appropriate.

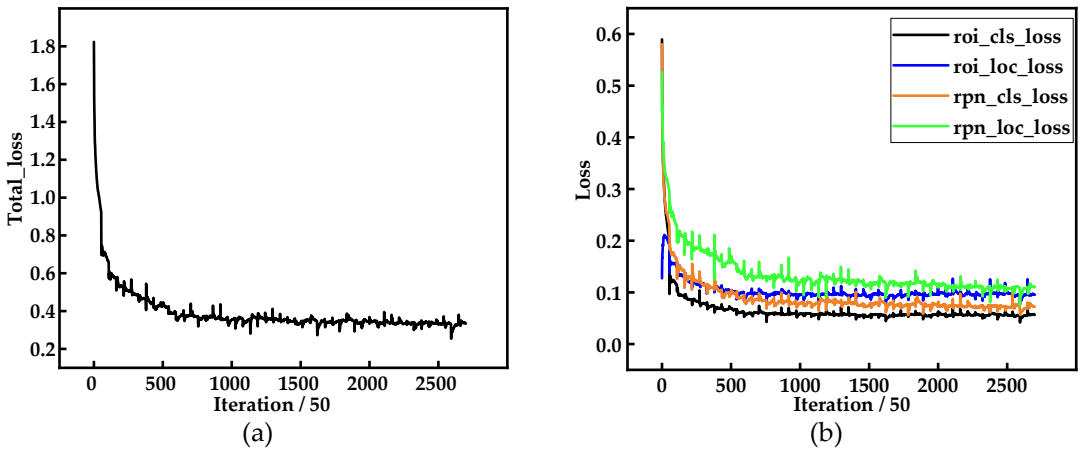

Figure 10. **(a)** The total_loss curve during the process of network training and **(b)** The roi_cls_loss, roi_loc_loss, rpn_cls_loss, rpn_loc_loss curves during the training.

5. Results and Discussion

After finishing the training of the network, we use 300 test images over 10 defect categories randomly chosen from the overall dataset to evaluate the multiscale defect detection network. We record the AP for the ten types of defects and the mAP. Then,

aluminum surface defect detection results output from the network are displayed. Lastly, we compute several saliency maps [29], specific to given images and classes, to represent the importance to the network at every location on input images.

5.1. mAP

Table 2. Performance comparison with different network.

Network	mAP(%)	Time(s/img)
Faster R-CNN	63.3	0.73
Multiscale Defect Detection Network	75.8	0.84

Table **Error! Reference source not found.** shows the mAP of Faster R-CNN and the multiscale defect detection network at test images. For Faster R-CNN, mAP is 63.3%, and the detection time is 0.73 second per image. For multiscale defect detection network, we achieve a mAP of 75.8%, and the large improvement of the network over Faster R-CNN illustrates that the idea of feature fusion promotes recognition accuracy on aluminum profile surface defects. Additionally, the detection time of the network is little more than Faster R-CNN, but the increase is not obvious and don't influence the defect detection.

The APs for ten types of defects of Faster R-CNN and multiscale defect detection network are shown in Figure **Error! Reference source not found.**. For Corner Leak(CL), Orange Peel(OP), Leakage, Crater and Parti-color(PC), both networks achieve high APs, nearly 100 percent. For Paint Bubble(PB) and Dirty Point(DP), the scale of which are small, APs of multiscale defect detection network is largely higher than Faster R-CNN, which illustrates the improvement of the network in the detection of small size defects. As can be seen in Table **Error! Reference source not found.** and Figure **Error! Reference source not found.**, the mAP of multiscale defect detection network and the APs for several types of defects are still low, so there are many defects that have not been detected. These missed inspection may be caused by the small training dataset. Therefore, in future studies, a larger dataset in each category will be generated to improve the network's detection capacity.

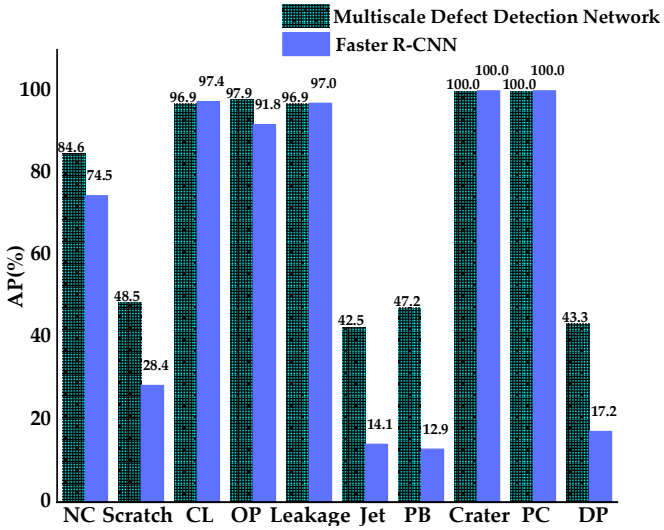

Figure 11. APs for ten types of defects of Faster R-CNN and Multiscale defect detection network.

Preprints (www.preprints.org) | NOT PEER-REVIEWED | Posted: 29 April 2019 doi:10.20944/preprints201904.0322.v1

Peer-reviewed version available at Materials 2019, 12, 1681; doi:10.3390/ma12101681

5.2. Aluminum surface defect detection results

Figure **12** shows the detection results of aluminum surface defect images using multiscale defect detection network. The position of the defects is marked by a green rectangular box, and the defect category and the confidence of the category are given in the upper left corner of the box.

Images with single type defect are shown in Figure **12**a, DP, PB, CL and OP are successfully detected. Besides, although DP scatters on the aluminum profile surface in Figure **12**a, almost all of them are detected, which indicates that the network has a strong detection capability in small size defects. In Figure **Error! Reference source not found.**b, we display the images with multiple type defects. Despite all defects are successfully recognized, the location of the rectangular boxes has some minor errors; for example, the box surrounding Non-conducting(NC) is too large, and the box positioning the scratch does not completely surround the scratch. These problems are related to incorrect location annotations of aluminum surface defect images.

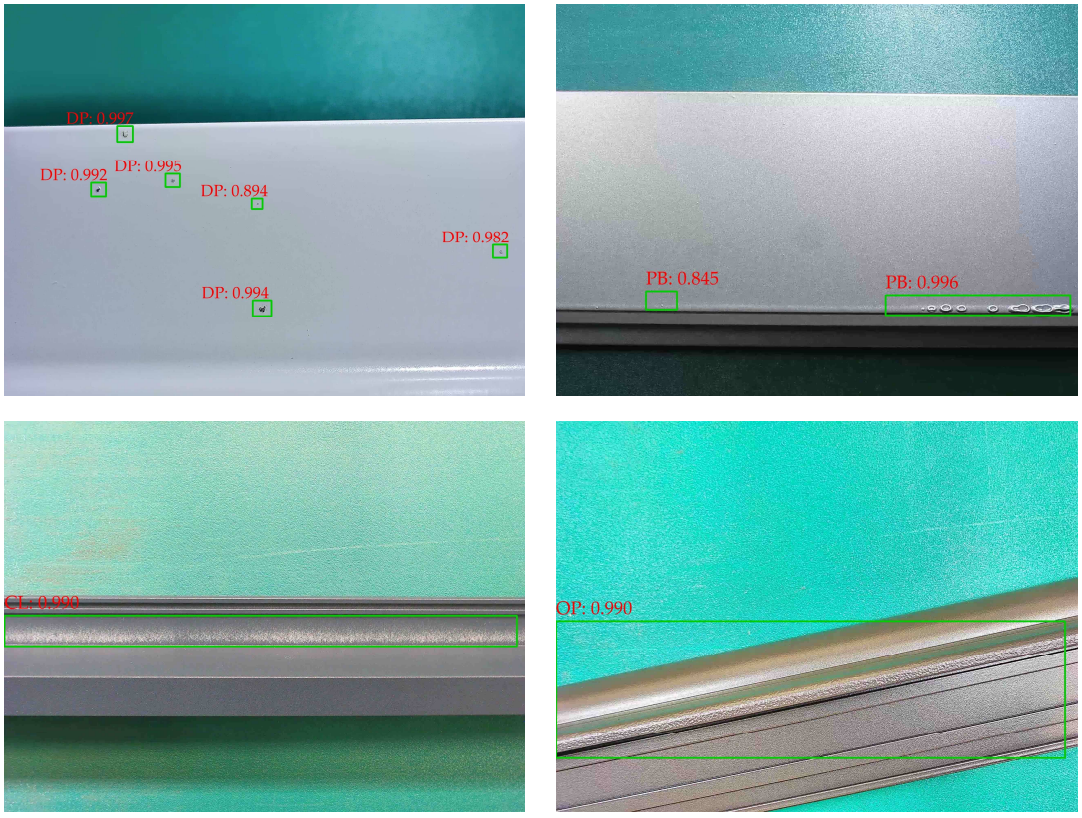

(a)

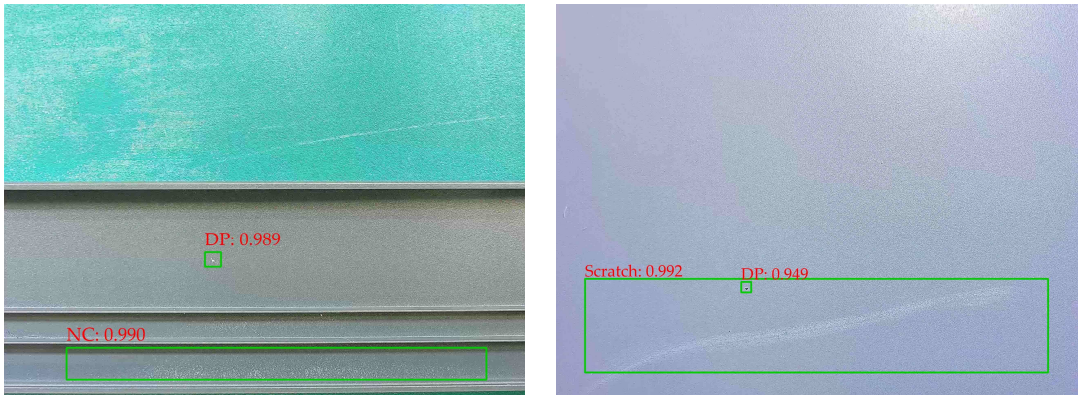

(b)

Figure 12. **(a)** Images wit single type defects; **(b)** Images with multiple types of defects.

5.3. Saliency Maps

A saliency map is an image that shows which pixels in the input image should be changed to affect the class score the most. Such pixels also are related to the defect location in the input image. Therefore, through the saliency map, it can intuitively analyze that multiscale defect detection network is interested in which part of the aluminum profile defect image, and thus can verify the effectiveness of the network. The saliency map is computed by the derivative of the loss of the classification layer with respect to the input image in the backward propagation. Detailed calculation of the saliency map can be seen in the paper by Simonyan *et al*. [29].

Figure **13** includes aluminum profile defect images and corresponding saliency maps. The defect images are shown in Figure **13**a, and red rectangular boxes roughly indicate the location of the defects. In Figure **13**b, we show the saliency maps in which the relatively bright place is the area where multiscale defect detection network focuses on. As can be seen in the figure, the focus of the network is on the aluminum profile, and the image background is selectively ignored. In addition, the brightness of the defect on the aluminum profile is particularly high in the saliency maps, indicating that the network mainly pay attention to the defects, which also confirms the effectiveness of the network.

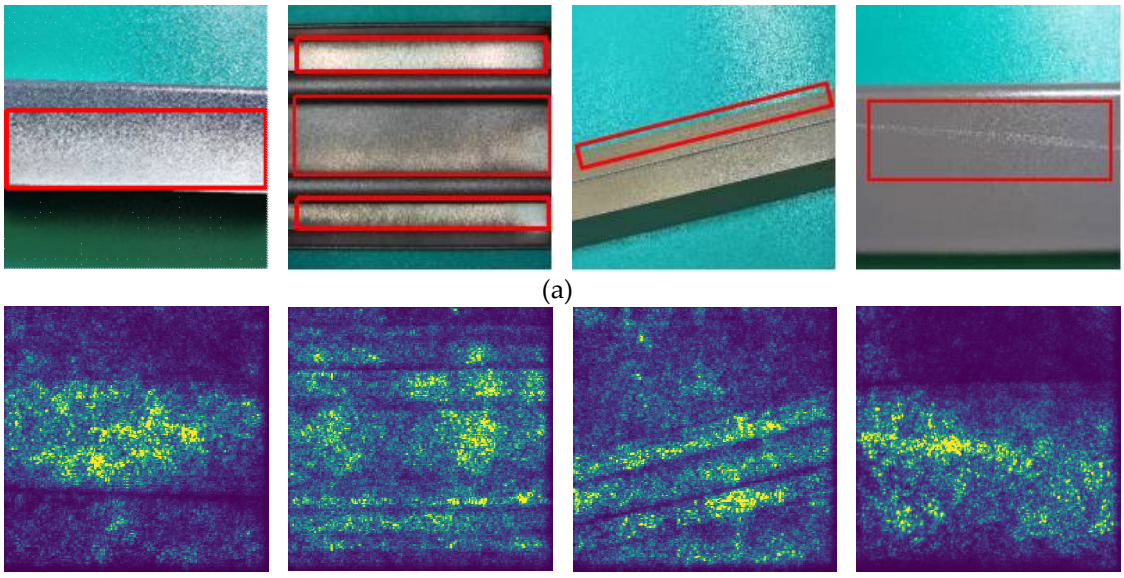

(a)

(b)

Figure 13. **(a)** Aluminum profile defect images; **(b)** Saliency maps.

6. Conclusions

Defects on aluminum profile surface will significantly influence the performance, reliability and safety of products. The artificial inspection is low precision and time consuming. Moreover, traditional machine vision-based defect detection methods overly rely on hand-crafted features which lack robustness and need to be carefully designed by experienced programmers. Therefore, in this paper, we propose a defect detection network based on deep learning which can automatically extract abstract and invariable features from large dataset, rather than designing low-level features artificially. The major findings of this paper can be summarized as follows:

(1) A multiscale defect detection network based on Faster R-CNN is proposed to recognize the aluminum profile surface defects. Considering the characteristics of defects on the aluminum profile surface, we add the idea of feature fusion to the basic Faster R-CNN to improve detection performances.
(2) The training images of aluminum profile surface defects are used to train the network. We adopt a data augmentation technique to expand the dataset. In the training process, we utilize the various losses to adjust parameters of the network.
(3) The performance of the trained multiscale defect detection network is evaluated on 300 test images. Compared with Faster R-CNN, the multiscale defect detection network achieve a higher mAP, which is 75.8%. For the small size defects(e.g. Paint Bubble and Dirty Point), the network get higher APs, which illustrates the effectiveness of the feature fusion. In addition, we display the detection results of aluminum profile surface defects images and the saliency maps which can verify the effectiveness of the network architecture.

In the future, more aluminum profile surface defects images in each category will be provided to train the network. In-depth analysis for the poor performance of the detection network in some types of defects will be performed, and the architecture will be improved.

Author Contributions: Conceptualization, Ruofeng Wei; Data curation, Ruofeng Wei; Formal analysis, Ruofeng Wei; Funding acquisition, Yunbo Bi; Investigation, Ruofeng Wei; Methodology, Ruofeng Wei; Project administration, Yunbo Bi; Resources, Yunbo Bi; Software, Ruofeng Wei; Supervision, Yunbo Bi; Validation, Ruofeng Wei; Visualization, Ruofeng Wei; Writing – original draft, Ruofeng Wei; Writing – review & editing, Yunbo Bi.

Funding: This research was funded by National Natural Science Foundation of China, grant number 51775495, and Science Fund for Creative Research Groups of National Natural Science Foundation of China, grand number 51821093.

Conflicts of Interest: The authors declare no conflict of interest.

Reference

1. Liu, Z.; Li, L.; Yi, J.; Li, S.; Wang, Z.; Wang, G. Influence of Heat Treatment Conditions on Bending Characteristics of 6063 Aluminum Alloy Sheets. *Trans. Nonferr. Met. Soc. of China* **2017**, *27*, 1498–1506. [CrossRef]
2. Bingöl, S.; Bozacı, A. Experimental and Numerical Study on the Strength of Aluminum Extrusion Welding. *Materials* **2015**, *8*, 4389-4399. [CrossRef][PubMed]
3. Liu, Z.; Li, L.; Li, S.; Yi, J.; Wang, G. Simulation Analysis of Porthole Die Extrusion Process and Die Structure Modifications for an Aluminum Profile with High Length–Width Ratio and Small Cavity. *Materials* **2018**, *11*, 1517. [CrossRef]
4. Tony W A. Automated inspection of metal products not quite ready for prime time. *Iron&Steel Maker* **1992**, *19*, 14-19.
5. Kong, X.; Li, J. Image Registration-Based Bolt Loosening Detection of Steel Joints. *Sensors* **2018**, *18*, 1000. [CrossRef][PubMed]
6. Kong, X.; Li, J. Vision-Based Fatigue Crack Detection of Steel Structures Using Video Feature Tracking. *Computer-Aided Civ. Inf.* **2018**, *33*, 783–799. [CrossRef]
7. Sun, X.; Gu, J.; Tang, S.; Li, J. Research Progress of Visual Inspection Technology of Steel Products—A Review. *Applied Sciences* **2018**, *8*, 2195. [CrossRef]
8. DuPont, F.; Odet, C.; Cartont, M. Optimization of the Recognition of Defects in Flat Steel Products with the Cost Matrices Theory. *NDT &E International* **1997**, *30*, 3–10. [CrossRef]
9. Yan, H. Prototype Optimization for Nearest Neighbor Classifiers Using a Two-Layer Perceptron. *Pattern Recogn.* **1993**, *26*, 317–324. [CrossRef]
10. Guo, J. H.; Meng, X. D.; Xiong, M. D. Study on Defection Segmentation for Steel Surface Image Based on Image Edge Detection and Fisher Discriminant. *J. Phys.: Conf. Ser.* **2006**, *48*, 364–368. [CrossRef]

11. Wu, G.; Kwak, H.; Jang, S.; Xu, K.; Xu, J. Design of Online Surface Inspection System of Hot Rolled Strips. In *2008 IEEE International Conference on Automation and Logistics*; 2008; pp 2291–2295.
12. Yazdchi, M.; Yazdi, M.; Mahyari, A. G. Steel Surface Defect Detection Using Texture Segmentation Based on Multifractal Dimension. In *2009 International Conference on Digital Image Processing*; **2009**; pp 346–350.
13. Ünsalan, C.; Erçil, A. *Automated Inspection of Steel Structures, Recent Advances in Mechatronics*; Springer Ltd.: Singapore, **1999**.
14. Krizhevsky, A.; Sutskever, I.; Hinton, G. E. ImageNet Classification with Deep Convolutional Neural Networks. *Commun. ACM* **2017**, *60*, 84–90. [CrossRef]
15. LeCun, Y.; Boser, B.; Denker, J. S.; Henderson, D.; Howard, R. E.; Hubbard, W.; Jackel, L. D. Backpropagation Applied to Handwritten Zip Code Recognition. *Neural Computation* **1989**, 1, 541–551. [CrossRef]
16. Deng, J.; Dong, W.; Socher, R.; Li, L. ImageNet: A Large-Scale Hierarchical Image Database. In *2009 IEEE Conference on Computer Vision and Pattern Recognition*; **2009**; pp 248–255.
17. Russakovsky, O.; Deng, J.; Su, H.; Krause, J.; Satheesh, S.; Ma, S.; Huang, Z.; Karpathy, A.; Khosla, A.; Bernstein, M.; et al. ImageNet Large Scale Visual Recognition Challenge. *Int. J. Comput. Vision* **2015**, *115*, 211–252. [CrossRef]
18. Girshick, R.; Donahue, J.; Darrell, T.; Malik, J. Rich Feature Hierarchies for Accurate Object Detection and Semantic Segmentation. *arXiv:1311.2524 [cs]* **2013**.[CrossRef]
19. Uijlings, J. R. R.; van de Sande, K. E. A.; Gevers, T.; Smeulders, A. W. M. Selective Search for Object Recognition. *Int. J. Comput. Vision* **2013**, *104*, 154–171.[CrossRef]
20. Cortes, C.; Vapnik, V. Support-Vector Networks. *Mach. Learn.* **1995**, 20, 273–297.[CrossRef]
21. Girshick, R. Fast R-CNN. *arXiv:1504.08083 [cs]* **2015**.[CrossRef]
22. Ren, S.; He, K.; Girshick, R.; Sun, J. Faster R-CNN: Towards Real-Time Object Detection with Region Proposal Networks. *arXiv:1506.01497 [cs]* **2015**.[CrossRef]
23. Lin, T.-Y.; Dollár, P.; Girshick, R.; He, K.; Hariharan, B.; Belongie, S. Feature Pyramid Networks for Object Detection. *arXiv:1612.03144 [cs]* **2016**.[CrossRef]
24. Guangdong Industrial Intelligence Big Data Innovation Competition. Available online: https://tianchi.aliyun.com/competition/entrance/231682/information(accessed on 17 September 2018).
25. Perez, L.; Wang, J. The Effectiveness of Data Augmentation in Image Classification Using Deep Learning. *arXiv:1712.04621 [cs]* **2017**.[CrossRef]
26. He, K.; Zhang, X.; Ren, S.; Sun, J. Deep Residual Learning for Image Recognition. *arXiv:1512.03385 [cs]* **2015**.[CrossRef]
27. Nair, V.; Hinton, G. E. Rectified Linear Units Improve Restricted Boltzmann Machines. In *Proceedings of the 27th International Conference on International Conference on Machine Learning*; ICML'10; Omnipress: USA, **2010**; pp 807–814.
28. Everingham, M.; Van Gool, L.; Williams, C. K. I.; Winn, J.; Zisserman, A. The Pascal Visual Object Classes (VOC) Challenge. *Int. J. Comput. Vision* **2010**, *88*, 303–338. [CrossRef]
29. Simonyan, K.; Vedaldi, A.; Zisserman, A. Deep Inside Convolutional Networks: Visualising Image Classification Models and Saliency Maps. *arXiv:1312.6034 [cs]* **2013**.[CrossRef]